OPTIMUM POWER FOR ER-70S-2 AND SS400 DISSIMILAR CDW JOINT

Djarot B. Darmadi*[1], Femiana Gapsari[1], Steamy Renergia Dirman[1], Marco Talice[2]

[1]Mechanical Engineering Department Brawijaya University, 65145, Indonesia
[2]PMSQUARED Engineering S.r.l.s, 09127, Italy

*b_darmadi_djarot@ub.ac.id

Selecting the right cutting tool material for the type of workpiece material plays a very important role in the machining process. The efficiency of the machining process is greatly influenced by this selection. The tables in the manuals or the manufacturer's instructions are commonly used documents for the selection of cutting tool materials. Within each of these document types, the cutting tool materials were described by different criteria. So, tool selection is considered as a multi-criteria decision-making activity. The values of the criteria for each type of cutting tool can be a number or a certain range. This study proposes a new method to rank and select cutting tools. First, a ranking of the solutions for each criterion will be performed. This ranking is based on the mean value of the criteria in each solution. Therefore, this method is called "Ranking the Solutions based on the Mean Value of Criteria - RSMVC". The RSMVC method was proven to be a highly reliable method for ranking the cutting tool materials. These results were successfully verified when solving the problems in different cases of cutter material selection.

Keywords: capacitive discharge welding, dissimilar metal welding joints, SCC resilience, SCC susceptibility, stress corrosion cracking

1 INTRODUCTION

Welding is the most effective and widely used joint method in technical applications. Since each combination of welding process and base metal has unique characteristics, parameter optimization is quite an interesting topic for both fusion [1–3] and solid-state welding [4-6]. One of the most relevant performance parameters to be evaluated is Stress Corrosion Cracking (SCC) resilience. The relevance of SCC resilience evaluation in assessing the welding joint integrity factor became evident with the pipeline incidents in Argentina [7] and Winnipeg, Canada [8]. In the published works that followed those events, researchers have identified metal corrosion and SCC resilience of the weld joints as the main leading factors to those incidents.
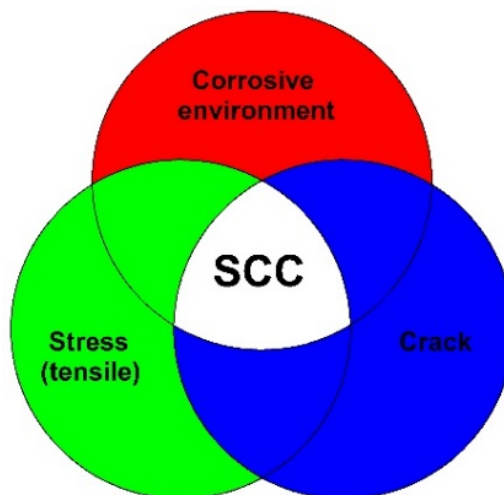

Figure 1. Stress Corrosion Cracking

SCC occurs when the three components of SCC, stress, corrosive environment, and cracks [9], are present together, as shown in Figure 1. Stress can manifest as either load stress or residual stress, the latter of which is typically high in the vicinity of the weld line. This residual stress always exists in the welding joint due to the ongoing non-uniform temperature in the welding process. The residual stress in resistance spot welding, which has a mechanism similar to that of CDW, is affected by welding parameters. It has been proven that with higher amperage, the residual stress will be lower for a variety of electrode forces and cycles [10]. The existence of voids in the weld joints, especially in CDW processes, can be difficult to avoid and may trigger a crack. Thus, two of the SCC's three components already exist in the weld joints, and when the weld joints are exposed to a corrosive environment, SCC can occur.

The SCC behavior of fusion welding has been investigated using both experimental and numerical approaches via quantitative and qualitative methods [11-17]. Kim et al. [11] studied the effect of residual stress on the SCC growth in GTAW joints. They measured SCC resilience as the time to failure and controlled residual stress by the number of welding passes. Their work proved that the fracture time decreases with increasing residual stresses. Kumar et al.

Journal of Applied Engineering Science

Vol. 21, No. 2, 2023
www.engineeringscience.rs

iipp
publishing

Djarot B. Darmadi et al. - Optimum power for ER-70S-2 and SS400 dissimilar CDW joint

[12] defined SCC resilience as the time to fracture of specimens exposed to the SCC environment. The measured yield strength of the TIG joint was 349.6 MPa, which is higher than the yield strength of the parent metal (284.2 MPa). When they exposed the specimen to vapors of 45% MgCl2 boiling at 155 °C, the time to failure of the welded joint was shorter than that of the parent metal. Darmadi et al. [13] improved the resilience to SCC loads of the Capacitive Discharge Welding Joint by varying the surface shape of the welded tips. The welded metals were steel and brass. The sharpening of one of the metal's surfaces, especially the steel's surface, significantly improved the joint SCC resilience.

Sepe et al. [14] evaluated the SCC behavior of GMAW joints of high strength steels when exposed to a NaOH 0.1M solution to simulate a pH = 8 environment and a pure H2SO4 solution to represent a pH = 4 environment. They evaluated the SCC by measuring the elongation loss rate (I□) and the area loss rate (I□). In the higher pH condition, the authors reported lower values of I□ and I□, which indicates that the SCC was less detrimental to the joints. Zhang et al. [15] studied the susceptibility of TIG joints, and the authors connected the SCC to the formed microstructure. They evaluated the SCC by its susceptibility indexes IR and I□, obtained via the Slow Strain Rate Test (SSRT). The authors report that lower residual strain level, a shorter fraction of Low Angle Boundaries (LABs), and smaller grain size result in higher SCC resilience. Their finding suggests that increasing the dislocation density and the □3 boundaries from the top to the root of the weld metal could increase the susceptibility to SCC. Zhang et al. [16] evaluated the crack tip heterogeneity of DMWJs using a numerical approach. On the base of the model, the authors concluded that the higher yield strength and hardening coefficient retain the SCC. Sun et al. [17] used a seven materials model to evaluate the cause of the SCC in the Dissimilar Metal Welding Joints (DMWJs). Using J integral, the authors have shown that the I-shape cracks present at the SA508 base metal zone and in the weld-metal have a detrimental effect on the SCC failure.

SCC behavior of solid-state welding has also been studied [18-20]. Parasuraman et al. [18] evaluated the SCC threshold of stir-welded AA7075-T651 aluminum joints. The authors found that the SCC threshold of the stir zone was lower than in the case of the base metal and explained their finding with the presence of finer grains in the stir zone. Cabrini et al. [19] stated that the load of the FSW process provides copper-rich precipitates at the borders of grains, which increases the SCC resiliences. The authors reported the development of localized applied strain and a lower tensile strength at the HAZ/TMAZ. It is a well-known fact that higher tensile strength and work hardening coefficient reduce the SCC driving force. Due to these contrasting effects, the susceptibility of the stir-welded AA-2024 joints and the base metal specimens show similar values. Qian et al. [20] improved the SCC behavior of FSW joints using Ultrasonic Impact Treatment (UIT). In their work, the SCC susceptibility was represented by ISSRT, and the authors found that using UIT, the ISSRT level was 0.129 lower than in the specimen without UIT, where the measured ISSRT level was 0.139. Wang et al. [21] evaluated the effects of thermal aging on the SCC susceptibility of wrought 316LN stainless steel. Thermal aging decreases the resilience to SCC of the 316LN stainless steel. Although the longer time of thermal aging does not alter the grain boundary size, it increases the disparity and the value of the hardness in the grain boundary due to the carbon enrichment. This carbon enrichment in turn increases the SCC susceptibility of the 316LN stainless steels.

In 2015, the CDW began to be utilized in the automotive industry in North America because of its advantages when compared to resistance welding when applied to hot-stamped boron steel [22]. Boron steel is widely used in the automotive industry due to its light weight and good crash properties. CDW allows for very quick energy release, which is stored slowly in the capacitor. Ketzel et al. studied the heat and temperature distribution of CDW [23]. The edge of the joint projection has very high temperatures, higher than the boiling point, while the center has much lower temperatures, causing lack of fusion. Magda et al. [24] evaluated three different CDW installations, namely KES 2100 from HBS and Soyer BMS-9. The loading voltage and capacitor capacitance were varied, and appearance and mechanical testing were applied to the joint. The optimal parameters for each machine were evaluated. It is reported that the optimal parameters for the KES 2100 and Soyer BMS-9 were 135 V, 88000□F and 165 V, 66000□F respectively.

This article studies the SCC (Stress Corrosion Cracking) behavior of CDW dissimilar metal joints. The SCC is measured as the time to failure. A welding parameter optimization (power) study is carried out to determine the joint's longest time to stand under an SCC load. This research is a continuation of previous published papers [25, 26] which discussed SCC and/or CDW respectively. The [25] is the first paper of us which discussed the SCC and the [26] is the SCC consideration when applied to the CDW joint. The parameter varied in the [26] was surface preparation, while in this paper it is power. Based on the previous report [22], the advantage of using CDW is better quality when applied to dissimilar metals, and in this report the ER-70S-2 and SS400 are used. ER-70S-2 is the filler metal wire, which will guarantee good coalescence of the joint while keeping the dissimilar metal as the topic of this paper.

2 EXPERIMENT SET UP

The CDW was applied using an electric welding heat source with adjustable variables. Figure 2 shows the special jig that was designed for this research. During the jig's operation, all welding parameters can be controlled and monitored to ensure compliance with desired working conditions during the welding process. The only parameter that changed during the experiments was the energy stored in the capacitor. Five different power levels were used in this experiment, namely 100, 130, 160, 190, and 220 Watts. The distance between the end grip of the wire and the plate was 5mm, commonly known as the Contact Tip to Work Distance (CTWD), and the weight of the upper jig, which

Journal of Applied Engineering Science

Vol. 21, No. 2, 2023

www.engineeringscience.rs

iipp
publishing

Djarot B. Darmadi et al. - Optimum power for ER-70S-2 and SS400 dissimilar CDW joint

holds the wire, was 4kg. The joined metals were an ER-70S-2 wire with a diameter of 2mm, and an SS400 steel strip, whose composition is shown in Table 1. The length of the wire was 5cm, but most of it was held by the upper grip, which acts as a cathode. The wire extension was 3mm. After all these parameters were set, the wire, with the upper grip, was dropped onto a 3mm SS400 strip, which was gripped by the lower jig. The strip is 15mm x 15mm x 3mm and acted as an anode. Once the two metals were in physical contact, a short circuit occurred and they released the stored power in the capacitor to melt the interface of both metals, forming a joint. The length of the wire was 5cm, but most of it is held by the upper grip, which acts as a cathode. The wire extension is 3mm. After all these parameters are set, the wire, with the upper grip, is dropped onto a 3mm SS400 strip, which is gripped by the lower jig. The strip is 15mm x 15mm x 3mm and acts as an anode. Once the two metals are in physical contact, a short circuit occurs and they release the stored power in the capacitor to melt the interface of both metals, forming a joint.
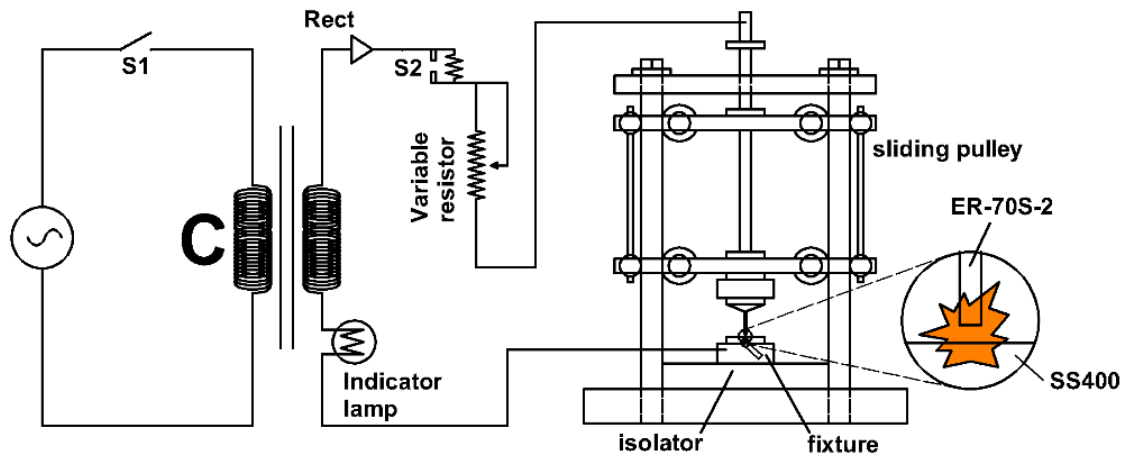

Figure 2. A CDW jig pertained for this research project

Table 1a. Chemical composition of ER-70S-2 (%)

C	Mn	Si	P	S	Ni	Cr	Mo	V	Cu	Ti	Zr	Al
0.07	0.9-1.4	0.4-0.7	0.025	0.035	0.15	0.15	0.15	0.03	0.5	0.05-0.15	0.02-0.12	0.05-0.15

Table 1b. Chemical composition of SS400 (%)

C	Mn	P	S
0.3 max	-	0.05 max	0.05 max

In this research, we studied the quality of CDW (Capacitor Discharge Welding) joints by examining their resilience to the Stress-Corrosion-Cracking phenomenon. It is believed, based on previous papers [11, 22-26], that power affects the SCC susceptibility in two ways: the quality of the resulting joint and the residual stress. As previously mentioned, we can define the SCC resilience as the joint's time to fail under given external loads. The independent parameters in the experiment are the applied external loads, and the dependent variable is the time to fail, while the electric power variation is considered as a treatment (independent variable). Although we take the external load as the independent variable, we cannot freely choose its value since the strength of the resulting joint sets a limit for the applicable external load. To predict the strength values of the resulting joints, we can use a rule of thumb that the highest dead load for the SCC test is about 70% of the joint ultimate tensile strength, followed by about 56%, 42%, 28%, and 14% of its ultimate tensile strength, respectively. Using this method, we can obtain a graph that reports the time to collapse as the dependent variable and the dead load as the independent variable, regardless of the varied joint strength obtained from varying the applied power. Figure 3 shows the jig used to carry out the SCC test. The CDW joint specimens were immersed in corrosive liquid (1 M hydrochloric acid (HCl)).
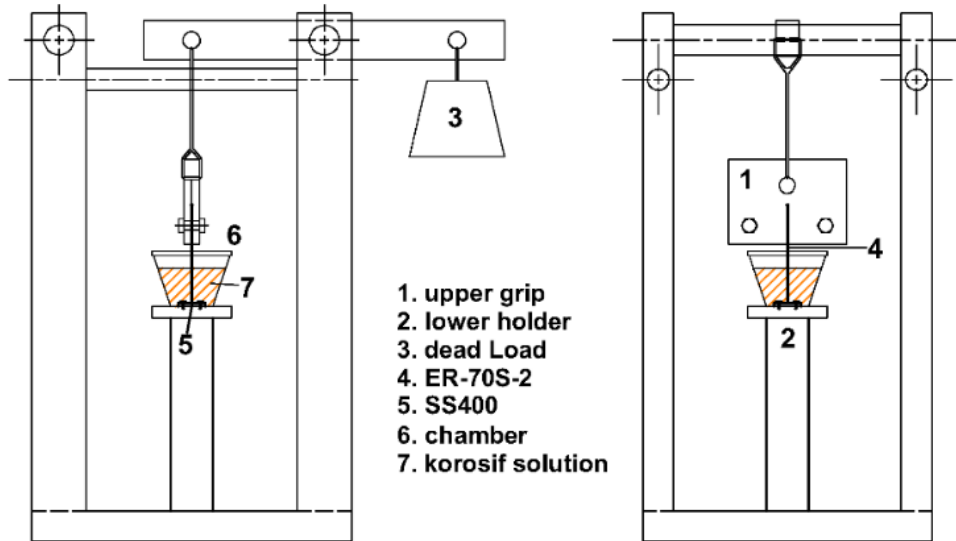
iipp
publishing

1. upper grip
2. lower holder
3. dead Load
4. ER-70S-2
5. SS400
6. chamber
7. korosif solution

Figure 3. SCC apparatus for the CDW joint

3 RESULTS AND DISCUSSION

The main result of this research is the Stress-Corrosion Resilience of the CDW joints produced. Stress-Corrosion Resilience is expressed as the time to fail under a given external dead load, as shown in Figure 4. For each power and external load, we have measured the time to fail of three specimens, i.e., Specimen 1, 2, and 3, respectively. It should be noted that in Figure 4, the time to fail is reported on the x-axis, while the dead load is on the y-axis. The measured mean values of time to fail are connected with black, red, blue, green, and yellow lines for the electric power of 100, 130, 160, 190, and 220 Watts, respectively. We then obtained the ultimate strength for each joint using the SCC test apparatus and gradually increasing the applied dead load value. The ultimate load values that brought the specimens to fail for the corresponding power of 100, 130, 160, 190, and 220 Watts were measured at 22.3kg, 36.9kg, 33.2kg, 23.3kg, and 19.8kg, respectively. Using a simple mechanical calculation, we can convert dead load values into ultimate stress values of 291.711 MPa, 474.072 MPa, 427.857 MPa, 304.202 MPa, and 260.485. If we take the 70%, 56%, 42%, 28%, and 14% of each load value and dip the specimens in the corrosive solution, we can compute the SCC resilience by measuring the time to fail of each specimen as shown in Figure 4.

In summary, Figure 4 shows that the 130 W specimen showed the highest SCC resilience. Under the application of a 10kg load, which translates into a stress value of s = 138.078 MPa, the 130W specimen can hold the SCC load for about 1219 minutes. The power varied to 220W, 100W, 190W, and 160W reduces the time to fail to 808, 335, 210, and 106 minutes, respectively.
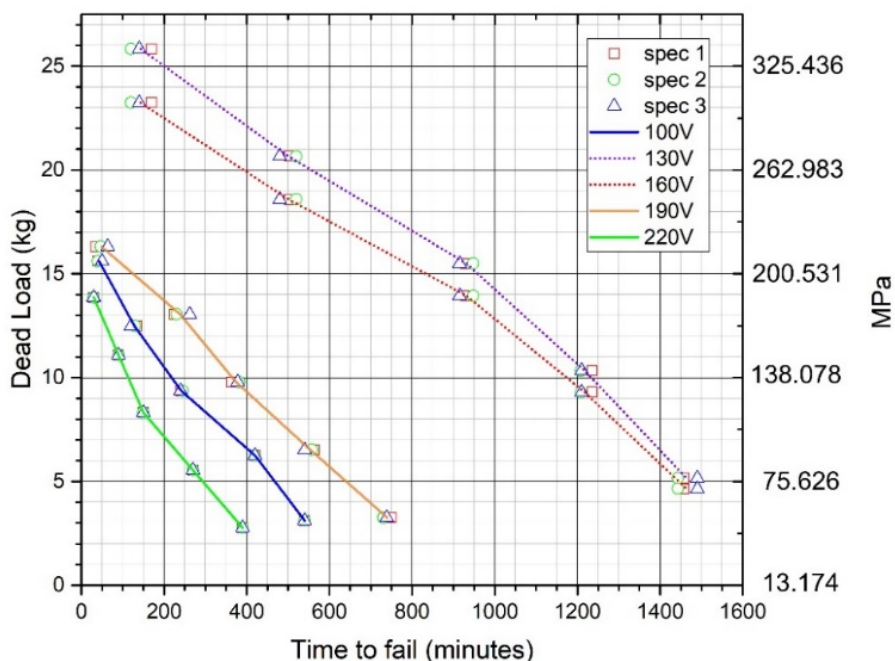

Figure 4. SCC resilience of CDW joints with varied voltage

Journal of Applied Engineering Science

Vol. 21, No. 2, 2023
www.engineeringscience.rs

iipp
publishing

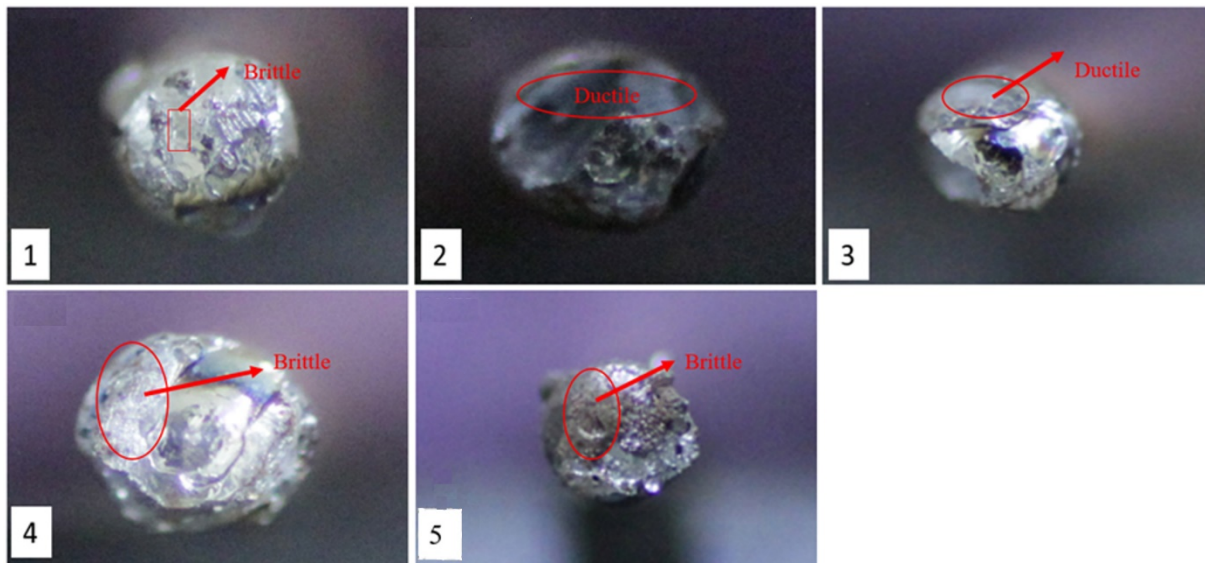*Djarot B. Darmadi et al. - Optimum power for ER-70S-2 and SS400 dissimilar CDW joint*

Figure 5. The fracture of the specimens when ultimate stress was applied

Supporting data were obtained from macro photos and SEM (Scanning Electron Microscope) images. Figure 5 shows the macro photos of the fracture surface. The fracture takes place in the area close to the weld joint, since it is always difficult to obtain perfect coalescence between two different metals in bimetal welding. Since Figure 5 is obtained using a conventional optical lens, the focus is very sensitive to the distance from the surface to the lens. Because the fracture surface is waving, the distance varies and not all of the fracture surface can be well captured. It should be noted that the diameter of the wire is 2mm, using this basic information the real size and the comparison between figures can be retrieved. The photos show that the fracture surface of the 130 Watt specimen is dominated by the presence of a ductile fracture (around 80% of the surface), followed by the 160 Watt specimen, which shows a ductile fracture that covers about 60% of its surface. We can identify the area affected by ductile fracture from the presence of dimples on the fracture surfaces [21]. Deeper and wider dimples indicate a more ductile joint. A ductile material has higher resilience, whilst one affected by a brittle fracture is more susceptible to the SCC load. From the same Figure 5, we can see that the 220 Watt, 100 Watt, and 190 Watt specimens are dominated by the presence of brittle fractures, which indicates a smaller fusion than in the 130 Watt and 160 Watt specimens. Generally speaking, the SCC fracture mode is of a brittle type [27], as shown in Figure 6e which shows a clear cleavage of brittle fracture that appears in the figure as shiny granular surfaces. These cleavages represent stress corrosion crack propagation, which has more than one source [27]. From the macro photos (Figure 5) of the brittle fracture, we can see that the crack grows discontinuously, and no crack branches are found.

To characterize the SCC, we have evaluated the microstructure of the fractured surfaces using SEM-EDS. SEM used dispersed electron to improve the captured image of the fracture surface by governs what is called as depth of field (D). The depth of field can be increased by minimizing the emission disc, aperture and magnifications, and it will be increased by longer working distance. Good surface readability will be obtained for the distance equal to best focus ± D/2. Figure 6 shows the SEM photo of all specimens which have been loaded with a 10 kg dead load (which corresponds to 138.078 MPa) and exposed to an SCC environment for 480 minutes and subjected to the ultimate loads. Table 2 summarizes the EDS results in the form of chemical content percentage. The existence of Cl and O shows that the corrosion takes place in the spot where EDS is applied. The Fe and O composition and the composition change of Cl show the existence of corrosion products in the spots where the EDS data have been taken. Using this method, we can estimate the area of corroded SCC load. Examining Figure 6, we can conclude that the extent of corrosive area increases when the applied power varies from 130, 160, 190, 100, and 220 Watt, respectively. This finding also corresponds to the sequence in the corrosion rates and confirms the results in terms of corrosion resilience already presented in Figure 4.
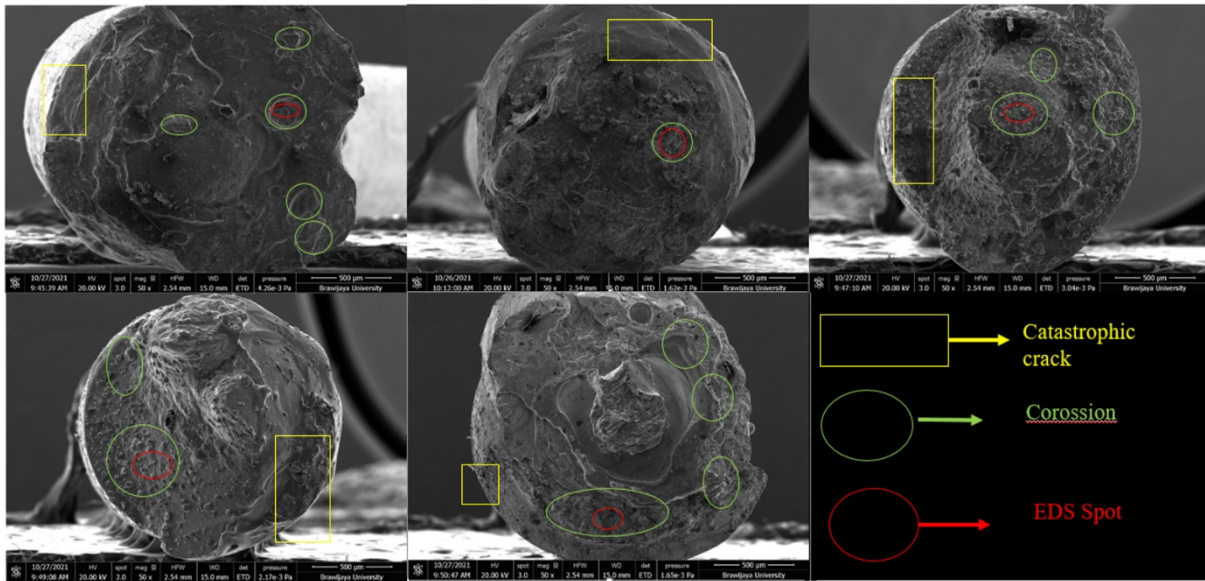
Figure 6. SEM photos of specimen's surfaces when exposed to the SCC load of 10kg in 480 minutes
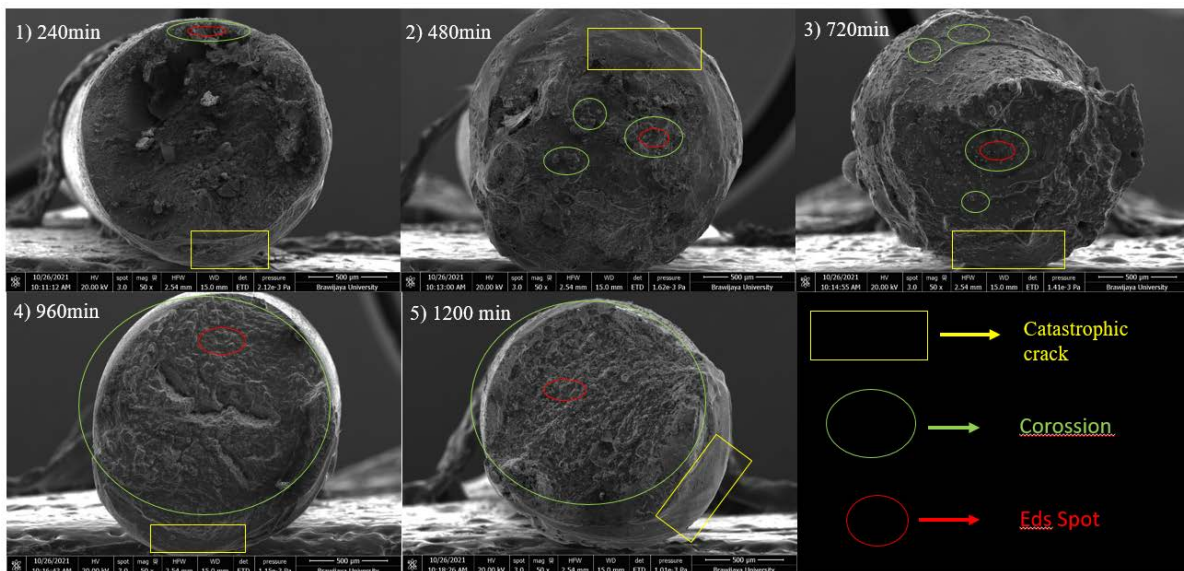

Figure 7. 130Watt specimen when exposed to SCC with 10kg dead load

Figure 7 shows the SEM photos of the 130 Watt case when the specimens are exposed to the SCC under an external load of 10 kg for 240, 480, 720, 960, and 1200 minutes. The application of the ultimate stress load follows the exposure of the joint at SCC condition. Using this method, we can obtain a fracture surface that comprises both the fracture surface due to the SCC load and the fracture surface due to the ultimate load. We focus our attention on the fracture surface due to the SCC load, which is shown by the corroded area. It should be noted that exposing the 130 Watt specimen to the SCC with an external load of 10 kg over 1200 minutes, almost equates to its SCC resilience, which is 1464 minutes (mean value). Using the described method, we can obtain the general idea of how the SCC crack develops in time, although we cannot obtain the SEM graph from a single specimen, which is impossible. Figure 6 shows the cleavages as the source of cracks while the specimens are dipped in the HCl solution. As it has been previously discussed, these cleavages represent Stress Corrosion Cracking with more than one source. Figure 6e clearly shows the existence of many cleavages as the crack source for the 220 Watt specimen [28, 29], which is suspected to be triggered by the welding voids. Analysis of the EDS results (table 2) of the oxygen content confirms the existence of corrosion. The presence of oxygen also indicates the formation of a passive oxide layer, and that the brittle fracture initiates the opening of a gap that allows the Cl atom to infiltrate formed cracks also allow the metal's cations (in this case is Fe+) to diffuse out, and promote the anions to penetrate the crack tips, which increases the SCC growth [30].

Table 2. EDS data when specimens exposed to SCC in 480 minutes

Specimen	Chemical Content on the eroded surface (%)			
	C	O	Cl	Fe
100W	14.99	24.42	4.16	55.06

Specimen	Chemical Content on the eroded surface (%)			
	C	O	Cl	Fe
130W	20.54	35.80	0.50	41.96
160W	0.23	29.24	1.54	67.55
190W	10.92	37.64	2.38	47.41
270W	8.19	17.76	0.40	69.35

Figures 6 and 7 show the catastrophic failure surfaces due to the ultimate load that forced the joint to break. Compared to when the specimens are exposed to the atmosphere, in the corrosive 1 M of HCL environment, the effect of stress concentration is exaggerated. In the welded joint with brittle fracture, the corrosive solution penetrates the shallow cleavages, and corrosion propagates to deeper and narrower regions. This promoted interaction with the corrosive environment causes catastrophic failure [31, 32].

4 CONCLUSION

We can conclude that the optimum power that produces the strongest joint is 130 Watt. All the performed tests show that the 130 Watt power brings optimum results from all examined aspects. The tensile strength of the joint using 130 Watt is 474.072 MPa which is 92.96% of the wire. Examination of the macrograph of the tensile test fractures shows that the fracture is dominated by ductile fracture, which indicates a good coalescence of the wire to the SS400 plate. Evaluation of the specimens' fracture surface under application of 10 kg of dead load in a corrosive environment for 8 hours shows that the corrosion develops less in the 130 Watt case. This trend remains consistent when the applied load is varied. The time to fracture due to the SCC of the 130 Watt specimen is always the longest, under any applied loads. In short, we can conclude that the optimum power for the CDW process using the provided jig is 130 Watt.

5 REFERENCES

[1] Srinivasa Reddy Vempati, K. Brahma Raju, K. Venkata Subbaiah (2018). Optimization of welding parameters of Ti6Al4V cruciform shape weld joint to improve weld strength based on Taguchi method. Materials Today: Proceedings 5, pp. 4948-4957.

[2] G. Satyanarayana, K.L. Narayana, B. Nageswara Rao (2019). Optimal laser welding process and expected weld bead profile for P92 steel. *SN Applied Sciences*, *1:1291*, https://doi.org/10.1007/s42452-019-1333-3.

[3] L.M. Ebhota and C.E. Etin-Osa (2021). Prediction of optimum weld tensile strength using response surface methodology. *European Journal of Engineering and Technology Research*, Vol. *6*, Issue *3*, pp. 146-149, http://dx.doi.org/10.24018/ejers.2021.6.3.2422.

[4] Xinjiang Fei and Zhifeng Wu (2018). Research of temperature and microstructure in friction stir welding of Q235 steel with laser-assisted heating. *Results in Physics*, *11*, pp. 1048 – 1051, https://doi.org/10.1016/j.rinp.2018.11.039.

[5] Ugrasen G, Bharath G, Kishor Kumar G, Sagar R, Shivu P R, Keshavamurthy R (2018). Optimization of process parameters for Al6061-Al7075 alloys in friction stir welding using Taguchi's technique. *Materials Today*, Proceeding *5*, pp. 3027-3035.

[6] Shuja Ahmed and Probir Saha (2020). Selection of optimal process parameters and assessment of its effect in micro-friction stir welding of AA6061-T6 sheets. *The International Journal of Advanced Manufacturing Technology*, Vol. *106*, 3045 – 3061, https://doi.org/10.1007/s00170-019-04840-6.

[7] C. Manfredi and J.L. Otegui (2002). Failures by SCC in buried pipelines. *Engineering Failure Analysis*, Vol.*9*, pp. 495-509, https://doi.org/10.1016/S1350-6307(01)00032-2.

[8] J. Wang and A. Atrens (2003). Microstructure and grain boundary microanalysis of X70 pipeline steel. *Journal of Material Science*, vol.*38*, pp.323-330, https://doi.org/10.1023/A:1021169700779.

[9] Djarot B. Darmadi, Natanael Ardi Sugiarto, Femiana Gapsari (2018). Stress corrosion cracking at ASTM A36 plate with varied grain orientation. *International Review of Mechanical Engineering*, vol. *12*, no. *12*, pp. 987-991, https://doi.org/10.15866/ireme.v12i12.16532.

[10] Y. Rihan, S. Ayyad and M.I. Elamy (2015). A study on the residual stresses in resistance spot welding. *Journal on Materials Science*, vol.3, pp. 26-30, DOI: 10.26634/jms.3.2.3504.

[11] Jae-Seong Kim, Bo-Young Lee, Woong-Gi Hwang, and Sung-Sik Kang (2015). The effect of welding residual stress for making artificial stress corrosion crack in the STS 304 pipe. *Advances in Materials Science and Engineering*, 7 pages. http://dx.doi.org/10.1155/2015/932512

[12] M. Vinoth Kumar, V. Balasubramanian, S. Rajakumar, Shaju K. Albert (2015). Stress corrosion cracking behaviour of gas tungsten arc welded super austenitic stainless steel joints. *Defence Technology*, vol. *11*, pp. 282-291. http://dx.doi.org/10.1016/j.dt.2015.05.009.

[13] Djarot B. Darmadi, Femiana Gapsari, Osmar Buntu Lobo and Firman Mangasa Simanjuntak (2020). Stress corrosion cracking threshold for dissimilar capacitive discharge welding joint with varied surface geometry. *Applied Sciences*, vol. *10*, 2180. DOI:10.3390/app10062180.

[14] R Sepe, F Bollino, F Caiazzo and F Berto (2021). Stress corrosion cracking behavior of welding joint of high strength steel. *IOP Conference Series: Materials Science and Engineering*, vol. *1038*, 012055. DOI:10.1088/1757-899X/1038/1/012055.

[15] Jingwen Zhang, Liming Yu, Zongqing Ma, Yongchang Liu, Chenxi Liu, Huijun Li, and Hui Wang (2020). Characterization of microstructure and stress corrosion cracking susceptibility in a multi-pass austenitic stainless steel weld joint by Narrow-Gap TIG. *Metallurgical and Materials Transaction A*, Vol. *51A*, pp. 4549 – 4562. https://doi.org/10.1007/s11661-020-05871-5.

[16] Shun Zhang, He Xue, Shuai Wang, Yuman Sun, Fuqiang Yang and Yubiao Zhang (2021). Effect of mechanical heterogeneity on strain and stress fields at crack tips of SCC in dissimilar metal welded joints. *Materials*, vol. *14*, 4450. https://doi.org/10.3390/ma14164450.

[17] Yuman Sun, He Xue, Kuan Zhao, Yubiao Zhang, Youjun Zhao, Weiming Yan, and Rehmat Bashir (2022). Cracking driving force at the tip of SCC under heterogeneous material mechanics model of safe end dissimilar metal-welded joints in PWR. *Science and Technology of Nuclear Installations*, 6605101, 10 pages. https://doi.org/10.1155/2022/6605101.

[18] Prabhuraj Parasuraman, Rajakumar Selvarajan, Balasubramanian Visvalingam, Rajkumar Ilamurugan and Kavitha Subra (2021). Stir zone stress corrosion cracking behavior of friction stir welded AA7075-T651 aluminum alloy joints. *Corrosion Reviews*, vol. *39*, no. *1*, pp: 55-62. https://doi.org/10.1515/corrrev-2020-0065.

[19] Marina Cabrini, Sara Bocchi, Gianluca D'Urso, Claudio Giardini, Sergio Lorenzi, Cristian Testa and Tommaso Pastore (2020). Stress corrosion cracking of friction stir-welded AA-2024 T3 alloy. *Materials*, vol. *13*, 2610. DOI:10.3390/ma13112610.

[20] Shuaihao Qian, Timing Zhang, Yuhua Chen, Jilin Xie, Yi Chen, Tiesong Lin, Hongxiang Li (2022). Effect of ultrasonic impact treatment on microstructure and corrosion behavior of friction stir welding joints of 2219 aluminum alloy. *Journal of Materials Research and Technology*, vol. *18*, pp. 1631 – 1642. https://doi.org/10.1016/j.jmrt.2022.03.068.

[21] Mingjia Wang, Lei Chen, Xiaocui Liu, Xiaocong Ma (2014). Influence of thermal aging on the SCC susceptibility of wrought 316LN stainless steel in a high temperature water environment. *Corrosion Science*, vol. *81*, pp. 117-124. http://dx.doi.org/10.1016/j.corsci.2013.12.011.

[22] Nigel Scotcmer (2015). The current rise in the use of capacitor discharge welding. *Welding Journal*, vol. 94, no. 2, pp. 32-36.

[23] Max-Martin Ketzel, Martin Hertel, Jorg Zchetzsche and Uwe Fussel (2019). Heat development of the contact area during capacitor discharge welding, *Welding in the World*, vol.63, no.5, pp. 1195-1203, DOI:10.1007/s40194-019-00744-x.

[24] A Magda, M Burca and M Lego (2018). Research regarding capacitor discharge stud welding with tip ignition on galvanized thin sheets, IOP Conf. Series: Materials Science and Engineering, vol. 416, ART 012015, DOI:10.1088/1757-899X/416/1/012015.

[25] Djarot B. Darmadi, Natanael Ardi Sugiarto, Femiana Gapsari (2018). Stress corrosion cracking at ASTM A36 plate with varied grain orientation. International Review of Mechanical Engineering, vol. 12, no. 12, pp. 987-991, DOI: 10.15866/ireme.v12i12.16532.

[26] Djarot B. Darmadi, Femiana Gapsari, Osmar Buntu Lobo & Firman Mangasa Simanjuntak (2020). Stress Corrosion Cracking Threshold for Dissimilar Capacitive Discharge Welding Joint with Varied Surface Geometry. Applied Sciences, vol. 10, no. 6, DOI: 10.3390/app10062180.

[27] Lin Shen, Hui Chen, Xiaoli Che, Yirong Wang (2020). Stress corrosion cracking behavior of laser-MIG hybrid welded 7B05-T5 aluminum alloy. *Corrosion Science*, Volume *165*, 108417, https://doi.org/10.1016/j.corsci.2019.108417.

[28] O. I. Zvirko, S. F. Savula, V. M. Tsependa, G. Gabetta, H. M. Nykyforchyn (2016). Stress corrosion cracking of gas pipeline steels of different strength. *Procedia Strutural Integrity*, vol. *2*, pp. 509 – 516, https://doi.org/10.1016/j.prostr.2016.06.066.

[29] ASM International (2006). Basic understanding of weld corrosion, *Corrosion of Weldments*.

[30] Ravindra Kumar (2021). Kinetics of oxidation and surface oxide cracking behaviours of weld metal and heat affected-zones of SMA weldment in thermal cyclic environment. *Materials Letters*, vol. *298*, 130042, https://doi.org/10.1016/j.matlet.2021.130042.

[31] Tongjiao Chu, Yanna Nuli, Haichao Cui, Fenggui Lu (2019). Pitting behavior of welded joint and the role of carbon ring in improving corrosion resistance. *Materials and Design*, vol. *183*, 108120. https://doi.org/10.1016/j.matdes.2019.108120.

[32] Nobphadon Suksangpanya, Nicholas A. Yaraghi, R. Byron Pipes, David Kisailus, Pablo Zavattieri (2018). Crack twisting and toughening strategies in Bouligand architectures. *International Journal of Solids and Structures*, vol. *150*, pp. 83-106. https://doi.org/10.1016/j.ijsolstr.2018.06.004.